Journal of Coastal Research	27	1	87–102	West Palm Beach, Florida	January 2011

Modeling Ocean Tides and Their Energetics in the North Patagonia Gulfs of Argentina

D. Moreira[†‡], C.G. Simionato[†‡], and W. Dragani[‡§††]

[†]Centro de Investigaciones del Mar y la Atmósfera (CIMA/CONICET-UBA)
Intendente Güiraldes 2160—Ciudad Universitaria
Pabellón II—2do. Piso
(C1428EGA) Ciudad Autónoma de Buenos Aires, Argentina
moreira@cima.fcen.uba.ar

[‡]Departamento de Ciencias de la Atmósfera y los Océanos FCEN, UBA
Intendente Güiraldes 2160—Ciudad Universitaria
Pabellón I—2do. Piso
(C1428EGA) Ciudad Autónoma de Buenos Aires, Argentina

[§]Servicio de Hidrografía Naval (SHN) and Escuela de Ciencias del Mar (ESCM–INUN)
Avda. Montes de Oca 2124
(C1270ABV) Ciudad Autónoma de Buenos Aires, Argentina

[††]Consejo Nacional de Investigaciones Científicas y Técnicas (CONICET), Argentina
Avda. Rivadavia 1917
(C1033AAJ) Ciudad Autónoma de Buenos Aires, Argentina

www.cerf-jcr.org

ABSTRACT

MOREIRA, D.; SIMIONATO, C.G., and DRAGANI, W., 2011. Modeling ocean tides and their energetics in the North Patagonia Gulfs of Argentina. *Journal of Coastal Research*, 27(1), 87–102. West Palm Beach (Florida), ISSN 0749-0208.

During the last decade, global tidal models have spectacularly improved. However, they still have difficulties in resolving tides over continental shelves and near coastlines. This study of tidal propagation from the continental shelf to the North Patagonia Gulfs of Argentina applies a set of three nested high resolution models based on the Hamburg shelf ocean model (HamSOM), where particular attention was paid to the bathymetry and the coast line. The study is complemented by the use of all the tidal gauge and tidal current observations available. Simulations display good agreement with observations, permitting the construction of higher resolution and more reliable cotidal and corange charts. The tidal regime in the area is essentially semidiurnal and dominated by M_2. This constituent propagates northward as a Kelvin wave and reaches the gulfs from the south. In their interior an important amplification is observed. Tidal currents are large at the mouths of the gulfs, and weaken toward their interior. The nonlinear transfer of energy from the semidiurnal to higher order harmonics was analyzed. This can be very important in the interior of the gulfs, particularly in Nuevo Gulf and in the northwestern San Matías Gulf, close to San Antonio. Energy flux and energy dissipation by bottom friction has been computed and indicate that this region dissipates 17% of the total energy dissipated on the Patagonian Shelf which, in turn, is one of the most dissipative areas of the world ocean. The Simpson-Hunter parameter computed from the simulations shows that in the mouth of the gulfs, particularly in San Matías and east of the Península de Valdés, the tides are energetic enough to overcome stratification and produce tidal fronts. The locations where tidal fronts are located are highly consistent with results from sea surface temperature and primary productivity data analyzed by other authors.

ADDITIONAL INDEX WORDS: *Tidal energetic, Patagonian Shelf, Argentina Continental Shelf, North Patagonia Gulfs.*

INTRODUCTION AND BACKGROUND

The Nuevo, San José, and San Matías gulfs, known as the North Patagonia Gulfs (Figures 1 and 2), are located on the Patagonian Argentinean Continental Shelf, in the southwestern Atlantic at approximately 42° S. The geometry and bathymetry of the area is complex, giving rise to a particular tidal dynamical response. The largest gulf, San Matías, communicates through a narrow mouth to the south with the smallest, San José, and through a broader mouth to the east with the open ocean. With an area of 19,700 km², San Matías is one of the largest gulfs in South America. Its depth reaches 200 m with two main depressions, the first one to the north and the second, to the south. Its mouth, 64 km wide, with depths shallower than 100 m, restricts the exchange with the shelf. The San José Gulf has an area of 814 km²; its east–west extension is 44.5 km, and it has a length of 18.5 km in the north–south direction. Its mouth, 6.8 km wide, is shallower than 80 m (SHN, 2000). With depths reaching 200 m and an area of 2200 km², the Nuevo Gulf is considered one of the best natural harbors of the world. This gulf is 56.3 km long and 40.2 km wide, and its mouth has a width of 11.2 km, connecting it to the southeast with the Patagonian Shelf.

The region is ecologically and economically important. Three harbors (San Antonio Oeste, San Antonio Este, and Punta Colorada) and two of the most important resorts of Argentina (Las Grutas and Playas Doradas) are located in the gulfs. One of the most important economic activities in the area is fisheries, and the gulfs have been declared a Wildlife Reserve by the United Nations Environmental Program (UNESCO, 1999) because of its unique marine fauna, which includes dolphins, sea lions, orcas, sea elephants, penguins, and whales, as well as a number of species of birds. The gulfs are also important for energy production via tidal power. Several projects have been outlined to profit from the large difference

DOI: 10.2112/JCOASTRES-D-09-00055.1 received 29 May 2009; accepted in revision 28 October 2009.

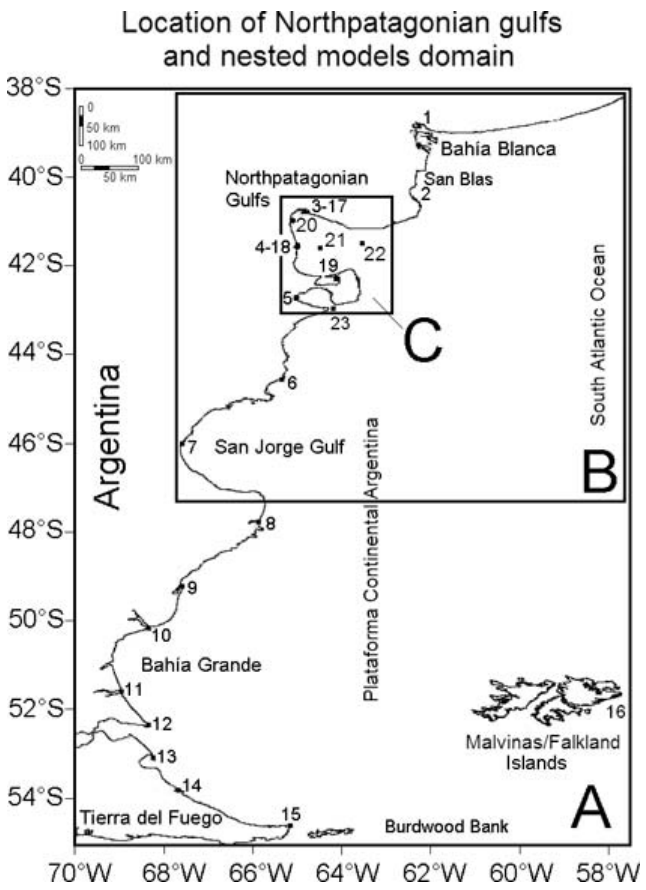

Figure 1. Map of the study area, showing the location of the North Patagonia Gulfs in the Patagonian Shelf and the domains of the three nested models (A, B, and C) used for their simulation. The dots and numbers display the location of the tidal gauge and current meter stations used to validate the simulations. The names and exact location of the stations indicated by the indices can be found in Table 1.

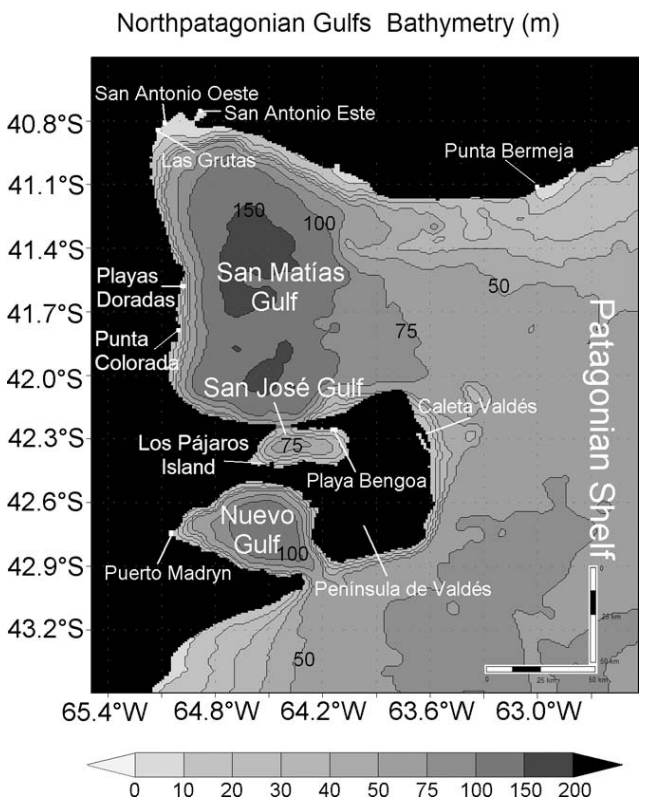

Figure 2. Bathymetry (isobaths in meters) of the North Patagonia Gulfs and main geographical references. The figure shows the domain of the lowest resolution model C.

in tidal amplitudes between San José and Nuevo gulfs (SOGREAH, 1959). Because most of those projects involve the construction of a channel between the two gulfs and given that they have different physical properties (Rivas and Beier, 1990), serious environmental impact could arise if a tidal power plant were eventually built in the area.

In spite of their ecological and economic importance, little is known about the physical oceanography of the gulfs, and particularly about their circulation and the forcings that produce circulation changes. Direct observations collected at the northeastern San Matías Gulf indicate weak mean currents of around 0.14 m s^{-1} at a depth of 25 m (Framiñan *et al.*, 1991). Nevertheless, tides in the region are among the largest in the world ocean, with ranges that exceed 8 m (SHN, 2008). In this macrotidal system, tidal currents tend to be larger than residual currents, having large effects on vertical mixing and on the spatial distribution of various parameters. In particular, the origin of several fronts observed in sea-surface–temperature satellite images of the region has been connected to tides (Bava *et al.*, 2002; Gagliardini and Rivas, 2004; Glorioso, 1987; Glorioso and Flather, 1995; Pisoni and Rivas, 2006; Rivas and Dell'arciprete, 2000). Those fronts are associated with areas of high primary production and have, therefore, large impact on fisheries (Romero *et al.*, 2006; Sabatini, 2004). They also have a large effect on determining the direction of CO_2 fluxes (Bianchi *et al.*, 2005).

Several works have emphasized the potential role of ocean tides on the mixing processes that maintain the thermohaline circulation (Egbert and Ray, 2000; Munk, 1997). An incompletely answered question is the amount of the energy dissipation by bottom friction, both in coastal areas and the deep ocean. Over the last years there has been a significant improvement in the acquisition of tidal data due in large part to the altimeter observations, and in global models due to improvements in resolution, parameterizations, data assimilation, and bathymetry (Lyard *et al.*, 2006). An example is the series of data assimilating finite element solutions (FES) models (Lefèvre *et al.*, 2002; Le Provost and Lyard, 1997; Le Provost *et al.*, 1998; Lyard, 1999; Lyard *et al.*, 2006). Nevertheless even the most advanced models still have difficulties in properly resolving the tides in coastal regions. This is due largely to the complex geometry of the basin, the limited knowledge of the bathymetry, and the still limited resolution (Lefèvre, Le Provost, and Lyard, 2000; Lyard *et al.*, 2006). In this sense, high resolution regional models, which incorporate detailed bathymetries, constitute a useful tool for improving

Table 1. *Locations of sea level gauge and current meters, and duration and sampling period of the series analyzed to obtain harmonic constants. Indices in brackets refer to locations in Figure 1. Sampling period of the current meter measurements was 30 minutes (index 17, 18, and 19) and 60 minutes (index 20, 21, 22, and 23).*

	Station (index)	Latitude	Longitude	Instrument	No. of Days of Observation
Tidal gauges	Puerto Belgrano (1)	38°53′ S	62°06′ W	Float	301
	San Blas (2)	40°33′ S	62°14′ W	Tide pole	38
	San Antonio Este (3)	40°48′ S	64°52′ W	Tide pole	40
	Punta Colorada (4)	41°46′ S	65°00′ W	Float	271
	Puerto Madryn (5)	42°46′ S	65°02′ W	Float	13505
	Santa Elena (6)	44°31′ S	65°22′ W	Tide pole	31
	Cdro. Rivadavia (7)	45°52′ S	67°29′ W	Float	1825
	Puerto Deseado (8)	47°45′ S	65°55′ W	Float	730
	San Julián (9)	49°15′ S	67°40′ W	Tide pole	45
	Punta Quilla (10)	50°07′ S	68°25′ W	Pressure sensor	180
	Río Gallegos (11)	51°36′ S	69°01′ W	Float	729
	Punta Vírgenes (12)	52°30′ S	68°28′ W	Tide pole	38
	Ba. San Sebastian (13)	53°10′ S	68°30′ W	Tide pole	61
	Río Grande (14)	53°47′ S	67°39′ W	Float	180
	Bahía Thetis (15)	54°38′ S	65°15′ W	Tide pole	139
	Puerto Argentino/Port Stanley (16)	51°42′ S	57°51′ W	Pressure sensor	1100
Current meters	San Antonio Este (17)	40°47′ S	64°53′ W	Aanderaa RCM9 MkII	25
	Punta Colorada (18)	41°41′ S	65°00′ W	Aanderaa RCM9 MkII	58
	Playa Bengoa (19)	42°15′ S	64°07′ W	Aanderaa RCM9 MkII	35
	Las Grutas (20)	40°56′ S	65°04′ W	Aanderaa, DCS 3900R	166
	San Matías Centro (21)	41°45′ S	64°32′ W	Mecabolier	12
	San Matías Boca (22)	41°37′ S	63°40′ W	Mecabolier	12
	Golfo Nuevo (23)	42°58′ S	64°12′ W	Aanderaa RCM5	149

our knowledge of tidal propagation in coastal areas with complex geometry and bathymetry, such as the North Patagonia Gulfs, and for making more accurate estimations of the involved energy dissipation rates (Lyard *et al.*, 2006). Very few studies have focused on the circulation of the North Patagonia Gulfs and their interactions. In the refereed literature, only two papers involving tidal propagation in the Nuevo Gulf by Mazio *et al.* (2004) and Mazio (2006) can be found. Several other models have been applied to the study of tidal propagation in the Patagonian Shelf (Glorioso, 2000; Glorioso and Flather, 1995, 1997; Glorioso and Simpson, 1994; Palma, Matano, and Piola, 2004; Simionato *et al.*, 2004). Nevertheless in those papers, horizontal resolution is coarser than 10 km, and consequently the bathymetric features of the gulfs, which determine tidal propagation in their interiors, are not well represented. As a result, little is known yet about tidal currents, the nonlinear interactions that probably occur in the area as a result of the complex geometry and bathymetry, and the energy dissipation in the region.

In the framework of the United Nations Development Program (UNDP, 2002), field measurements and numerical simulations were undertaken with the aim of overcoming this limitation. This article, as a contribution to this project, aims to study tidal propagation from the continental shelf to the North Patagonia Gulfs and the interactions between them, nonlinear generation of higher order harmonics, energy dissipation by bottom friction, and tidal fronts. For that purpose, a set of high resolution (1 km × 1 km) numerical simulations was performed, in which particular attention is put on the bathymetry and the coastline. The model used is the three-dimensional Hamburg Shelf ocean model (HamSOM), by Backhaus (1983, 1985) at the Institut für Meereskunde (IfM) in Hamburg, Germany. Numerical solutions were validated with all the tidal gauge and tidal currents observations available, and given that M_2 is by far the most important constituent (Glorioso and Flather, 1997), only its propagation is discussed here.

DATA

The locations along the Patagonian coast where sea level and currents have been measured are listed in Table 1 and shown in Figure 1. The table also presents information about the instrument used, the number of days of observation, and the sampling period. Those data were used to compute the harmonic constants presented in this article using the Foreman (1977, 1978) routines. Most of the data were kindly provided by the Servicio de Hidrografía Naval of Argentina. We also used the M_2 amplitude and phase values from Woodworth *et al.* (2005) in the Malvinas–Falkland Islands station Puerto Argentino–Port Stanley (index 16 in Figure 1) and the tidal current observations from Moreira *et al.* (2009).

NUMERICAL SIMULATIONS

Simulations Description

The HamSOM model, applied in our simulations, has been described in many publications (Alvarez Fanjul, Pérez Gómez, and Rodríguez Sanchez−arévalo, 1997; Backhaus, 1983, 1985; Backhaus and Hainbucher, 1987), and the reader is referred to them for further details about its formulation and parameterizations. The approach has been to perform three-dimensional simulations of the tidal propagation, even when density has been kept constant. Even though tides are barotropic, an advantage of using a multilayer model is to allow for a better representation of bottom friction. In HamSOM, bottom stress is

Table 2. *Amplitude and Greenwich phase lag of the tidal constituent M_2 observed at coastal stations, values derived from the numerical simulations, difference between them, and the observed values and vector differences. The last two columns are the amplitude and phase lag of the M_2 ocean tidal loading computed from FES2004 (Lyard et al., 2006). The location of the stations can be observed in Figure 1 and Table 1 by their index.*

M_2 Constituent	Observed		Model A				Model B				Model C				Tidal Loading	
Station (index)	Amp. (m)	Phase Lag (°)	Amp (m)	Phase Lag (°)	Diff. Amp	Diff. Phase Lag	Vect. Diff. (m)	Amp (m)	Phase Lag (°)	Diff. Amp	Diff. Phase Lag	Vect. Diff. (m)	Amp (m)	Phase Lag (°)	Diff. Amp	Diff. Phase Lag	Vect. Diff. (m)	Amp (m)	Phase Lag (°)
San Blas (2)	0.82	159	0.75	168	*0.07*	*−9*	*0.14*	0.90	158	*−0.08*	*1*	*0.08*	—	—	—	—	—	*0.00*	*46*
San Antonio Este (3)	3.14	72	2.96	92	*0.18*	*−20*	*1.07*	3.38	81	*−0.24*	*−9*	*0.56*	*3.14*	*77*	*0.00*	*−5*	*0.27*	*0.01*	*236*
Punta Colorada (4)	2.84	63	2.74	88	*0.10*	*−25*	*1.21*	3.05	75	*−0.21*	*−12*	*0.65*	*3.00*	*75*	*−0.16*	*−12*	*0.63*	*0.01*	*230*
Puerto Madryn (5)	1.89	320	1.74	350	*0.15*	*−30*	*0.95*	1.85	337	*0.04*	*−17*	*0.55*	*1.87*	*337*	*0.02*	*−17*	*0.55*	*0.01*	*146*
Santa Elena (6)	1.63	269	1.46	294	*0.17*	*−25*	*0.69*	1.63	280	*0.00*	*−11*	*0.31*	—	—	—	—	—	*0.02*	*86*
Cdro. Rivadavia (7)	2.06	220	1.95	250	*0.11*	*−30*	*1.03*	2.20	236	*−0.14*	*−16*	*0.61*	—	—	—	—	—	*0.01*	*52*
Puerto Deseado (8)	1.79	139	1.69	147	*0.10*	*−8*	*0.26*	—	—	—	—	—	—	—	—	—	—	*0.01*	*309*
San Julián (9)	2.83	75	3.14	82	*−0.31*	*−7*	*0.48*	—	—	—	—	—	—	—	—	—	—	*0.02*	*233*
Punta Quilla (10)	3.74	52	3.59	64	*0.15*	*−12*	*0.78*	—	—	—	—	—	—	—	—	—	—	*0.03*	*217*
Río Gallegos (11)	3.85	45	4.20	40	*−0.35*	*5*	*0.50*	—	—	—	—	—	—	—	—	—	—	*0.03*	*199*
Punta Vírgenes (12)	3.20	7	3.85	18	*−0.65*	*−11*	*0.94*	—	—	—	—	—	—	—	—	—	—	*0.04*	*185*
Ba. San Sebastián (13)	3.29	352	3.68	10	*−0.39*	*−18*	*1.16*	—	—	—	—	—	—	—	—	—	—	*0.03*	*171*
Río Grande (14)	2.62	333	2.99	342	*−0.37*	*−9*	*0.57*	—	—	—	—	—	—	—	—	—	—	*0.03*	*158*
Bahía Thetis (15)	1.27	299	1.30	290	*−0.03*	*9*	*0.20*	—	—	—	—	—	—	—	—	—	—	*0.02*	*126*
Puerto Argentino/Port Stanley (16)	0.44	275	0.43	272	*0.01*	*3*	*0.03*	—	—	—	—	—	—	—	—	—	—	*0.02*	*112*

parameterized by means of a quadratic law in terms of the horizontal velocity vector at the bottom layer of the model and the vertically averaged horizontal velocity in a frictional layer close to the bottom (see, for example, Simionato *et al.*, 2004).

Following the approach of Alvarez Fanjul, Pérez Gómez, and Rodríguez Sanchez-Arévalo (1997) and Simionato *et al.* (2004) who used the same model to study the tidal propagation along the Spanish and Patagonian coasts, respectively, the astronomical forcing is neglected in the interior of the model domain. Even though some authors handle the self-attraction and loading of the ocean tide by a simple scalar multiplier of the elevations in the momentum equations (Accad and Pekeris, 1978), this is only a crude approximation, and it is particularly poor in near-coastal areas (Francis and Mazzega, 1990). We evaluated these effects at the location of the coastal tidal stations of Table 1 and in sections across the shelf and the North Patagonia Gulfs by integrating the loading Green's function utilizing the FES2004 global model (Bos and Scherneck, 2008). Values for the ocean tidal loading amplitude and phase lag of the M_2 constituent are given in the last column of Table 2. It can be observed that, in general, amplitudes are very small, on the order of a few centimeters. It reaches its maximum at Punta Vírgenes, where the loading is around 0.04 m for an observed M_2 tidal amplitude of 3.20 m and a simulated value of 3.85 m. In the North Patagonia Gulfs, values are even smaller, not exceeding 0.02 m. The computation in other points of the gulfs (not shown) demonstrated that for M_2 tidal loading amplitude is always less than 0.025 m and represents, therefore, approximately 0.5% of the modeled tidal amplitude. We can conclude, consequently, that ignoring the ocean tidal loading constitutes a minor error that does not essentially modify the results of this work.

Given that the mouths of the North Patagonia Gulfs are very narrow, a high spatial resolution (on the order of 1 km) is required to properly solve the detail of the complicated geometry. Because both the global and regional models available for the Patagonian continental shelf have a resolution too low to provide adequate boundary conditions for a small scale model of the gulfs, especially in those areas close to the coast, it was necessary to extend the model domain to permit the free propagation of the tidal wave to the region of interest. To reduce the computational cost, we decided to apply a hierarchy of three nested models of progressively higher resolution, hereafter referred to as domains A, B, and C, respectively, and illustrated in Figure 1.

The largest scale domain A, with a horizontal resolution of 9 km, covers the whole Patagonian Shelf from 55° S to 38.3° S and from 69.4° W to 57.5° W and provides sea surface elevation boundary conditions every half hour of simulation to the intermediate scale model B. With a horizontal resolution of 3 km, this second domain spans 38.4° S and 47.5° S, and 68.1° W and 58.4° W and, in turn it gives boundary conditions to the smallest scale model C. This last model has a horizontal resolution of 1 km and covers the area between 43.5° S and 40.5° S and 65.5° W and 62.4° W (Figure 1).

The bathymetric data used to construct the grids were obtained by digitization of nautical charts from the Argentine Hydrographic Service (Borjas and Dragani, 2004). To ensure the adequate definition of the complex coast line, we also used

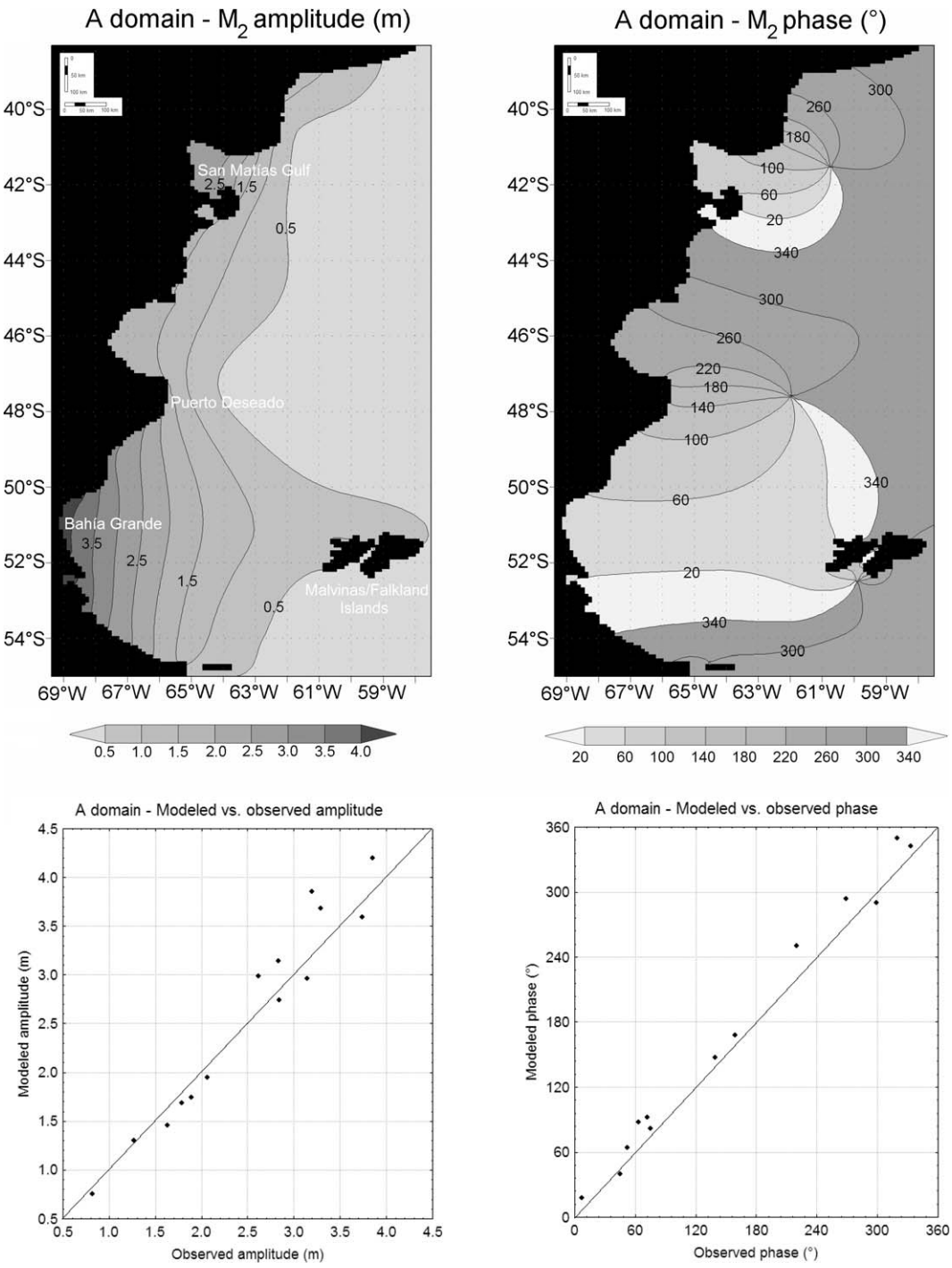

Figure 3. Upper panels: Corange (amplitudes in meters) and cotidal (Greenwich phase lags in degrees) maps of the M_2 constituent from model A. Lower panels: Scatter plots of modeled *vs.* observed amplitudes and Greenwich phase lags for model A.

high resolution data from the Global Self−consistent, Hierarchical, High−resolution Shoreline Database (GSHHS) of the National Geophysical Data Center (NGDC−NOAA) (Wessel and Smith, 1996). The bathymetry for the smallest scale domain C is shown in Figure 2.

The tidal amplitude and phase lag boundary conditions for the lowest resolution model A come from lower resolution numerical solutions from simulations performed with HamSOM covering the whole Argentinean Continental Shelf (Simionato *et al.*, 2004). That model, in turn, was forced at

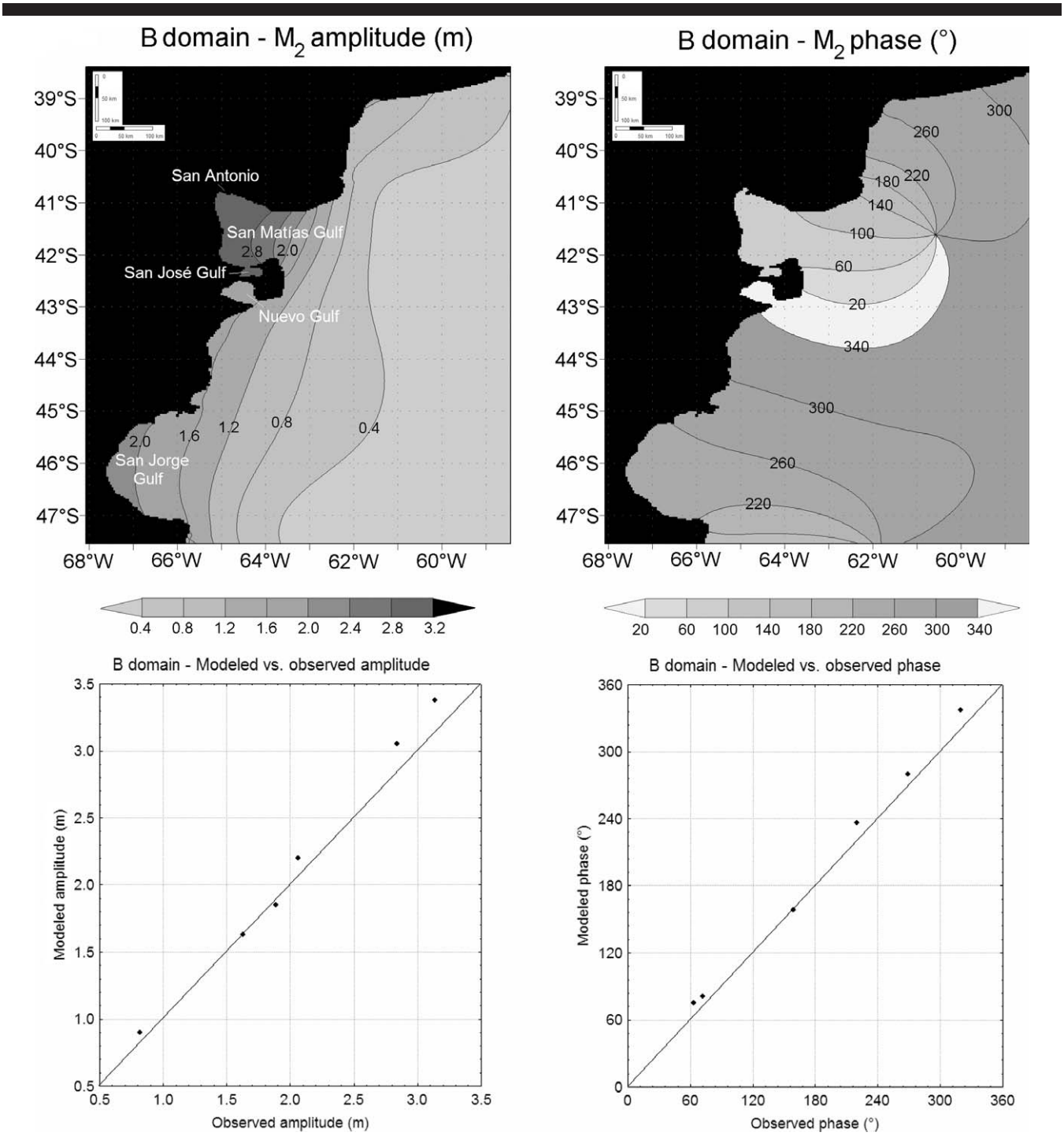

Figure 4. Upper panels: Corange (amplitudes in meters) and cotidal (Greenwich phase lags in degrees) maps of the M_2 constituent from model B. Lower panels: Scatter plots of modeled *vs.* observed amplitudes and Greenwich phase lags for model B.

the boundaries with values derived from the global model of Zahel (1997). Even though the discussion in this paper is mostly oriented to M_2 and the higher order harmonics derived from it, the eight most important tidal constituents were included in the simulations: M_2, S_2, N_2, K_2, K_1, O_1, P_1, and Q_1.

Model A has 10 vertical layers, chosen according to the characteristic depth of the area and to ensure a proper description of the upper part of the ocean in future runs forced by winds. Layers have bottoms at 10, 20, 40, 60, 100, 200, 500, 1000, 3000, and 6000 m. Because the model is a *z*-coordinate

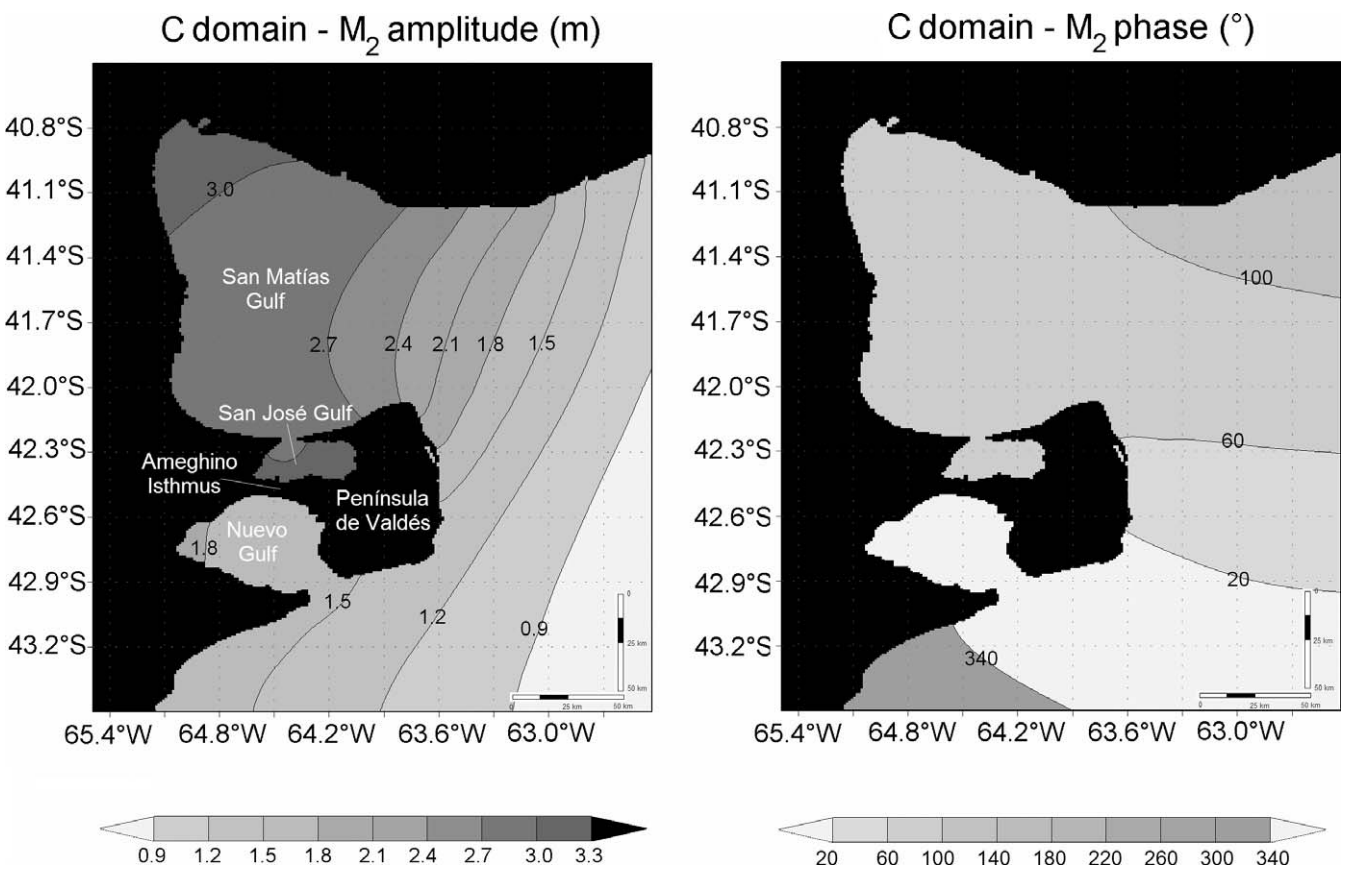

Figure 5. Corange (amplitudes in meters) and cotidal (Greenwich phase lags in degrees) maps of the M_2 constituent from model C.

one, the minimum depth allowed, to prevent the first layer from drying out, was 5 m. The time step was 600 seconds, in compliance with the Courant, Friedrich, and Lewy or CFL criterion (Courant *et al.*, 1928), and the coefficient of horizontal eddy viscosity was 50 $m^2\ s^{-1}$. Simionato *et al.* (2004) showed that the tidal wave is not sensitive to this parameter in HamSOM on the Argentinean continental shelf. The simulation was started from rest, and a ramp-up with a duration of 1 day was applied to the boundary conditions to avoid an excessive production of inertia-gravity waves at the beginning of the simulation and, therefore, to reduce the overall spin-up time. The model was run for a total of 14 months. Nevertheless, to ensure the stability of the solutions, we only used the last 12 months in the analysis. Sea surface elevations and currents were saved at every grid point every half hour.

The solution for the sea surface elevation derived from model A was used as a boundary condition for model B every half hour, with a linear interpolation at the intermediate time steps. The use of the total sea surface instead of tidal amplitudes and phase lags in the simulation has the advantage of allowing the propagation from one to another domain of the higher order harmonics resulting from nonlinear interactions, such as M_4. Model B has 10 vertical layers with depths at 10, 20, 30, 50, 75, 100, 200, 500, 1000, and 2000 m, and the minimum depth permitted is 4 m. The horizontal eddy viscosity coefficient was 15 $m^2\ s^{-1}$ and the time step 300 seconds. The model was run for the same period and under similar conditions to the previous one.

Finally, the higher resolution model C was forced at the boundaries with sea surface elevation data every half an hour coming from model B. The C domain also has 10 vertical layers with bottoms at 10, 20, 30, 40, 50, 75, 100, 125, 150, and 175 m. The horizontal eddy viscosity coefficient was 5 $m^2\ s^{-1}$ and the time step 300 seconds. The model was run for the same period and under similar conditions to the previous one.

Once the simulations were completed, a harmonic analysis was performed using the Foreman (1977, 1978) routines to obtain the amplitude and phase lag of every tidal constituent and the tidal ellipses at every grid point.

Modeled Amplitudes and Phase Lags

A comparison of the amplitudes and phase lags of the M_2 constituent observed at the tidal stations (Figure 1) and those derived from the simulations in the three domains is shown in Table 2. All the available coastal stations were considered except Puerto Belgrano (Bahía Blanca), where the tidal gauge is installed at the interior of a harbor that cannot be properly represented by the resolution of model A. The table shows the agreement between observed and simulated values in both

Table 3. *Amplitude and Greenwich phase lag of the tidal constituent M_4 observed at coastal stations, values derived from the numerical simulations, difference between them and observed values, and vector differences. The location of the stations can be observed in Figure 1 and Table 1 by their index.*

M_4 Constituent	Observed		Model A				Model B				Model C				
Station (index)	Amp (m)	Phase Lag (°)	Amp (m)	Phase Lag (°)	Dif. Amp.	Dif. Phase Lag	Vector Diff. (m)	Amp (m)	Phase Lag (°)	Dif. Amp.	Dif. Phase Lag	Vector Diff. (m)	Amp (m)	Phase Lag (°)	Dif. Amp.	Dif. Phase Lag	Vector Diff. (m)
S. Antonio Este (3)	0.05	244	0.05	187	*0.00*	*57*	*0.05*	0.05	184	*0.00*	*60*	*0.05*	0.06	172	−0.01	72	0.06
Punta Colorada (4)	0.02	163	0.03	200	*−0.01*	*−37*	*0.02*	0.04	191	*−0.02*	*−28*	*0.02*	0.04	190	−0.02	−27	0.02
Puerto Madryn (5)	0.18	238	0.15	249	*0.03*	*−11*	*0.04*	0.12	237	*0.06*	*1*	*0.06*	0.14	246	0.04	−8	0.05
Cdro. Rivadavia (7)	0.10	155	0.14	206	*−0.04*	*−51*	*0.11*	0.13	206	*−0.03*	*−51*	*0.10*	—	—	—	—	—
Puerto Deseado (8)	0.08	287	0.07	5	*0.01*	*−78*	*0.09*	—	—	—	—	—	—	—	—	—	—
San Julián (9)	0.14	164	0.08	176	*0.06*	*−12*	*0.06*	—	—	—	—	—	—	—	—	—	—
Punta Quilla (10)	0.22	131	0.18	153	*0.04*	*−22*	*0.08*	—	—	—	—	—	—	—	—	—	—
Río Gallegos (11)	0.21	89	0.20	94	*0.01*	*−5*	*0.02*	—	—	—	—	—	—	—	—	—	—
Punta Vírgenes (12)	0.06	331	0.13	2	*−0.07*	*−31*	*0.08*	—	—	—	—	—	—	—	—	—	—
Río Grande (14)	0.15	219	0.15	241	*0.00*	*−22*	*0.06*	—	—	—	—	—	—	—	—	—	—

amplitudes and phase lags, which improves as the model resolution increases. The differences in the amplitude for model A are, in general, on the order of 10% except for Punta Vírgenes, where the model overestimates the amplitude by 20%. Differences in phase lag are less than 30° in every case. For model B the differences in the amplitude were less than 10% and in the phase lag, less than 17°. Model C shows a much better approximation than model A in both amplitude and phase lag to the few observations available in that area, but its performance in this aspect is similar to model B.

To allow for a better visualization of the results, we show in the lower panels of Figures 3 and 4 simulated *vs.* observed amplitude and phase lag for the domains A and B. The correlation was 0.97 for the amplitude and 0.99 for the phase lag in model A and 0.99 for both variables in model B. It can be seen in the figure that even though model A does not exhibit a systematic trend to overestimation or underestimation of the amplitude, it tends to overestimate the phase lag by an average of 10°. Similarly, model B overestimates the phase lag by an average of 6°. The figure illustrates the good quality of the simulations and their potential value to studies of the extensive areas of the Patagonian Shelf where observational data are not available.

The cotidal and corange map of the M_2 constituent derived from the solution of model A is shown in the upper panels of Figure 3. As in previous works (Glorioso and Flather, 1997; Simionato *et al.*, 2004), it can be observed that the tide propagates along the Patagonian Shelf as a Kelvin wave with amplitudes that reach their maxima at the coast and decrease offshore. Maximum amplitudes occur around Bahía Grande, with values of more than 4 m. The cotidal map shows three amphidromic points located eastward of San Matías Gulf, east of Puerto Deseado, and south of the Malvinas–Falkland Islands, also in good agreement with the simulations by other authors.

The results corresponding to model B are shown in Figure 4. The main feature is the large amplification of the tide in the northwest of San Matías Gulf, reaching values of more than 3 m, in agreement with the tidal information available for San Antonio (SHN, 2008). The tidal amplitude is maximum inside the San Matías and San José gulfs, whereas it has much lower values in the San Jorge and Nuevo gulfs.

Figure 5 shows maps derived from the simulation with the highest resolution model C. The amplification of the tide as it propagates from the Patagonian Shelf to the interior of the gulfs is particularly noticeable in the San José and Nuevo gulfs, inside of which amplitude grows by 10% over that observed at the mouths. As a result, M_2 reaches amplitudes of more than 3 m in the whole interior of the San José Gulf and in the western area of the San Matías Gulf. In Nuevo Gulf, amplitudes are smaller, reaching up to 1.8 m. Noticeable also is the difference in the tidal phase lag between the San José and San Matías gulfs, to the north, and the Nuevo Gulf, to the south, of around 100°. This results because the tide propagates northward; therefore, it takes longer to reach the interior of the San Matías and, especially, the San José gulfs, than the Nuevo Gulf. This feature, known from observations (SHN, 2008), resulted in the proposal to utilize the narrow Ameghino Isthmus separating Península de Valdés from the continent

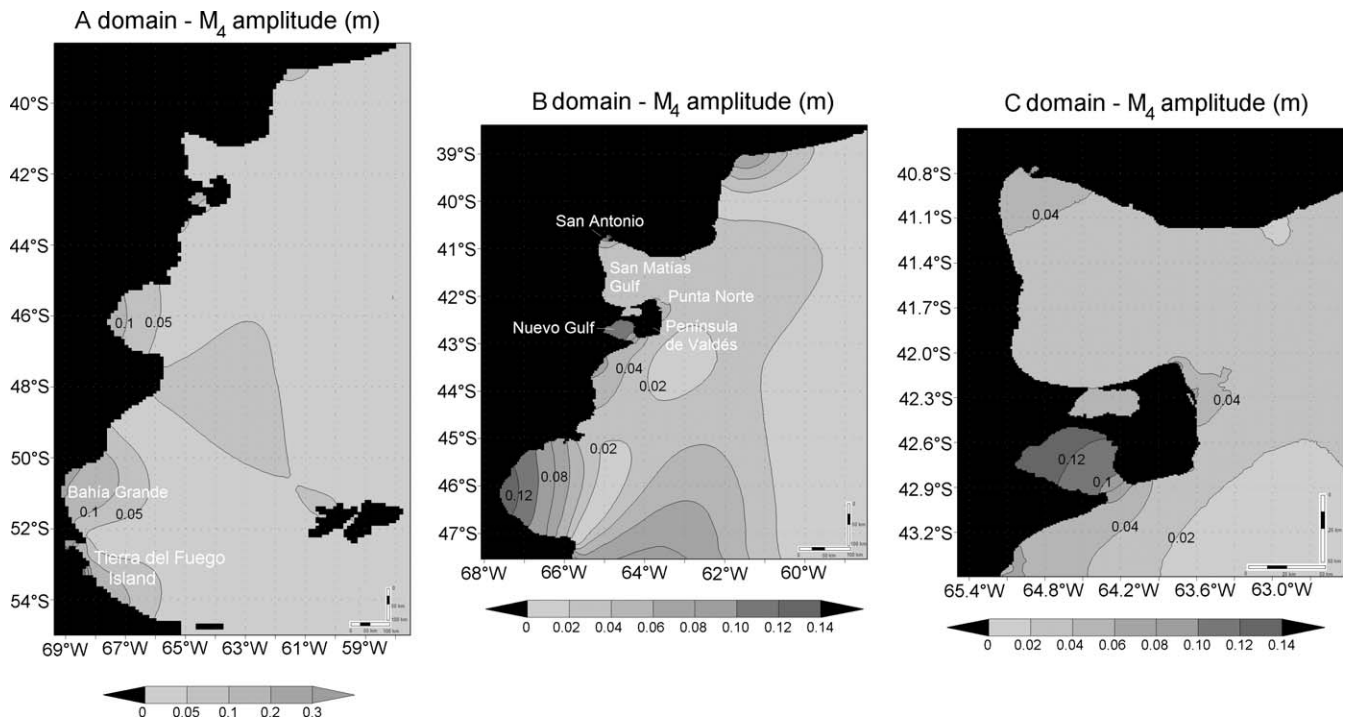

Figure 6. Corange (amplitudes in meters) maps of the M_4 constituent from models A (left panel), B (central panel), and C (right panel).

to build a channel connecting the San José and Nuevo gulfs for energy generation (SOGREAH, 1959).

Table 3 shows the amplitude and phase lag of M_4 derived from observations at coastal stations and those obtained from the simulations. Errors are in general larger than those found for M_2 (Table 2). For model A, the correlation between observed and modeled amplitudes was 0.88, and for phase lags, it was 0.91. For models B and C, the number of observations is too low to allow the computation of the correlation coefficient.

Figure 6 shows the corange charts for the M_4 constituent derived from the simulations in the three domains. This figure reveals that nonlinear effects are important along the Patagonian coast. In the A domain, the largest amplitudes are observed eastward of Tierra del Fuego Island and Bahía Grande, where the values are as high as 0.35 m. In the B domain, the largest amplitudes for this constituent occur at Nuevo and San Jorge gulfs, where values exceed 0.12 m. In the interior of the North Patagonia Gulfs, nonlinear interactions are very important, particularly in the region close to San Antonio (northwesternmost portion of San Matías Gulf) and in the whole Nuevo Gulf. Figure 6 also displays regions of high nonlinear interactions at Punta Norte (northeast of the Península de Valdés).

Tidal Currents

To validate the currents resulting from the simulations, we compared M_2 HamSOM–generated tidal ellipses with measurements made in the San José, San Matías, and Nuevo gulfs. Results are shown in Figure 7. Their correspondence can be observed in the figure, the model being able to capture both the speed and direction of the currents. Differences in phase lag were less than 8° and in amplitude less than 20%, except at Playa Bengoa and the interior of San Matías Gulf, where tidal currents are weak.

The left panel of Figure 8 shows the M_2 ellipses corresponding to the uppermost level of model A. Largest currents occur in the following areas: along the coast from Tierra del Fuego to San Jorge Gulf, over the Burdwood Bank, northwest of the Malvinas–Falkland Islands, and at the San Matías Gulf mouth. These results compare very well with those from Simionato *et al.* (2004), who applied HamSOM with a much lower resolution to describe currents in the region. Although correspondence with the Glorioso and Flather (1997) results are, in general, similar to what was found by Simionato *et al.* (2004), the simulations here have weaker currents between Bahía Blanca and San Blas. The central panel of Figure 8, derived from the solution of model B, shows in a greater detail that maximum speeds generally occur in the inner shelf and, especially, in association with significant changes in the coast line orientation. This last feature is particularly evident northeast of the Penínula de Valdés and south of the San Jorge Gulf. The right panel of Figure 8 shows the M_2 tidal ellipses derived from the smallest scale model, C. A significant reduction of the tidal currents toward the interior of the North Patagonia Gulfs is observed, compared with the large values at their mouths. Maxima occur northeast of the Península de Valdés. In agreement with the observations, even though the

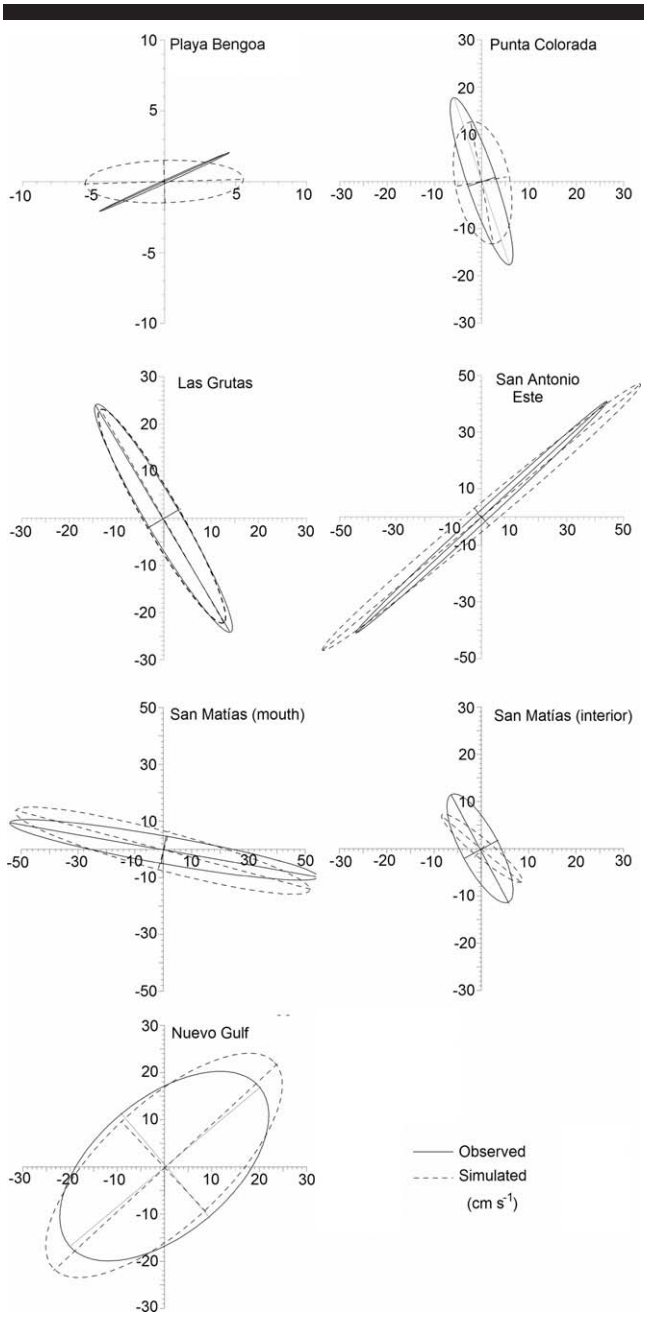

Figure 7. Comparison of measured (solid line) and computed (dotted line) M_2 tidal ellipses at different locations in the North Patagonia Gulfs.

speed of the currents in San Matías Gulf is much weaker in the interior than at the mouth, it increases northward along the coast, reaching values of more than 0.6 m s^{-1} near San Antonio. However, speeds at the mouth, particularly north and east of the Península de Valdés, can reach two and even three times those values. Also in agreement with the few observations available, speeds in the interior of Nuevo and San José gulfs are much weaker than at their mouth.

Tidal Energetics

Additional important quantities that can be calculated from our simulations are the energy flux and the dissipation by bottom friction. Given the good correspondence between simulated and observed harmonic constants for both sea level and tidal currents, it is expected that a good estimation of those quantities will derive from model results. No estimation of those parameters is available in the literature for the North Patagonia Gulfs.

The energy flux was computed following Pugh (1987). This formulation was used by Glorioso and Flather (1997) and Simionato *et al.* (2004) to estimate the energy flux over the Patagonian shelf from tidal simulations of the most important tidal constituents, in the former, and of M_2, in the latter. Glorioso and Flather (1997) concluded that in this region the energy flux due to M_2 dominates, being two orders of magnitude larger than the ones due to the other constituents. The results of our work support that finding.

The M_2 energy flux on the Patagonian Shelf as derived from model A is shown in the left panel of Figure 9. This figure is similar to that derived by Simionato *et al.* (2004), but there are some differences from those presented by Glorioso and Flather (1997). The energy enters the region mainly from the south and reaches the shelf through the region between Tierra del Fuego and the Burdwood Bank. Another flux branch reaches the Malvinas–Falkland Islands from the northeast. West of the islands, this branch turns to the west and joins the main flux at approximately 52° S. Then it flows northward and dissipates along the coastline as it reaches the San Matías Gulf. The most important differences with respect to the Glorioso and Flather (1997) simulations are the flux incoming from the northeast to the Malvinas–Falkland islands and a maximum of the flux over the Burdwood Bank, both features being absent in the previously mentioned paper.

The M_2 flux diminishes northward, reaching very small values north of San Matías Gulf, indicating that almost all of the energy is dissipated along the Patagonian Shelf. To identify the most important areas for dissipation and to quantify its magnitude, we derived the mean rate of energy dissipation per unit area by bottom friction following Davies, Sauvel, and Evans (1985). Results for the Patagonian Shelf (right panel of Figure 9) are mostly consistent with the Simionato *et al.* (2004) and Glorioso and Flather (1997) derivations. Dissipation in the region is large and highly localized in four main regions: over the Burdwood Bank, east of Tierra del Fuego, south of the San Jorge Gulf, and at the San Matías Gulf mouth. Secondary dissipation areas are found north of the San Jorge Gulf and around the Malvinas–Falkland Islands. The main difference with the former computations by Glorioso and Flather (1997) is the lack in our results of dissipation between San Blas and Bahía Blanca. Nevertheless, this feature is consistent with the low energy flux observed over the area, not only in our simulations but in those of Simionato *et al.* (2004) and Glorioso and Flather (1997).

An integration of the M_2 energy dissipation by bottom friction over the model domain results in 87 GW (1 GW = 10^9 W). Cartwright and Ray (1989) obtained for the Patagonian Shelf a value of, 245 GW; Egbert and Ray (2000), 120 GW;

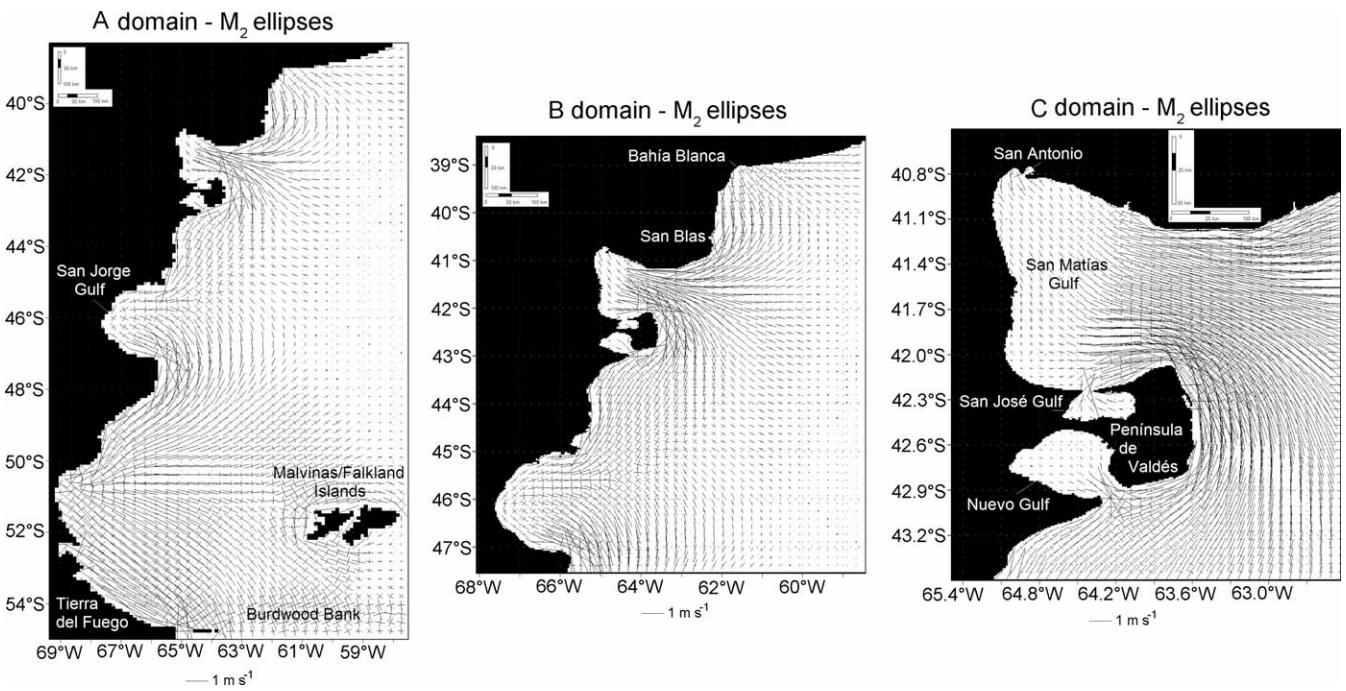

Figure 8. M_2 tidal current ellipses derived from models A (left panel), B (central panel), and C (right panel).

Glorioso and Flather (1997), 218 GW; Miller (1966), 130 GW; Palma, Matano, and Piola (2004), 82 GW; and Simionato *et al.* (2004), 117 GW, even though it must be taken into account that in every case the domains and constituents included in the analysis are different. The previous simulation in which the area considered for the estimation of the dissipation is most similar to ours is the one by Palma, Matano, and Piola (2004), who obtained a value of 82 GW, comparable with our 87 GW. In any case, dissipation in the region constitutes an important amount of the estimated total global value 2420 GW (Le Provost *et al.*, 1998).

Figure 10 shows the energy flux corresponding to M_2 and the energy dissipation by bottom friction derived from model B. In this figure the features previously described can be better observed, including the concentration of dissipation areas southward of San Jorge Gulf and at the mouth of San Matías Gulf. Little energy flows into Nuevo and San José gulfs, consistent with the low speeds suggested in their interior (Figure 8). This last feature can be better observed in Figure 11, which shows the results of model C. Results indicate that the energy flux toward the North Patagonia Gulfs comes from the south and flows parallel to the coast. A significant amount of energy enters from the south of San Matías Gulf, flows westward reaching the deep parts of the western gulf where it turns eastward, and then exits along the north sector of the mouth. The narrow mouths of the San José and Nuevo gulfs restrict energy flow into their interiors. The higher resolution of model C (Figure 11) confirms that energy dissipation in the North Patagonia Gulfs is mainly concentrated in two areas, one northeast of the Península de Valdés and the other one east of Caleta Valdés. These regions, in turn, correspond to areas where currents speeds reach relative maxima (Figure 8). An integration of the energy dissipation by bottom friction for the model C domain amounts to 15 GW, representing 17% of the total dissipated on the shelf (87 GW in our simulations), showing the importance of the gulfs in that aspect.

Tidal Fronts

A last contribution that our simulations can provide is an estimation of the possible locations of tidal fronts on the Patagonian Shelf using the Simpson-Hunter parameter. According to the Simpson and Hunter (1974) theory, the location of tidal fronts produced by mixing depends upon the rate between the potential energy due to vertical mixing and the dissipation of kinetic energy due to tidal currents. Different authors have applied different critical values for this parameter, indicating that the dissipated energy is able to destroy stratification and, consequently, define the location of the front. Values of the critical parameter are normally between 2 and 3 (Glorioso and Flather, 1995; Hearn, 1985; O'donnell, 1993; Palma, Matano, and Piola, 2004); in our case we have chosen 2.5.

Figure 12 shows the Simpson-Hunter parameter estimated from the results of simulations A, B, and C. Regions where its value is less than 2.5, where tides produce large vertical mixing, are shaded. Tidal fronts occur in areas where energy dissipation is at a maximum: east of Tierra del Fuego, south of San Jorge Gulf, and at the San Matías Gulf mouth. The simulations with the highest resolution model C show in greater detail the frontal regions at the mouth of San Matías

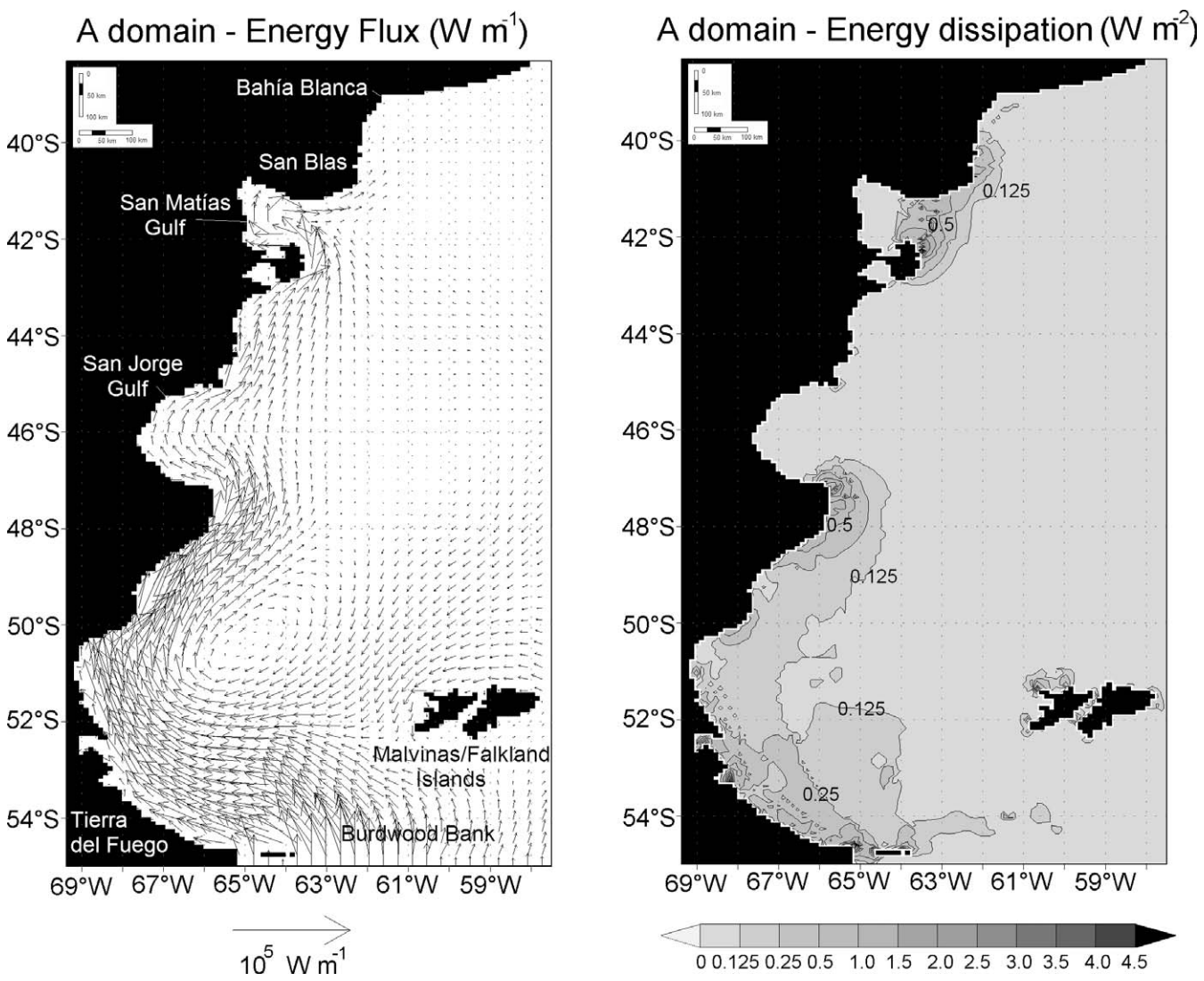

Figure 9. M_2 tidal energy flux vectors in W m^{-1} (left panel) and contours of tidal energy dissipation by bottom friction in W m^{-2} (right panel) derived from model A. Note that the contour interval is not regular.

Gulf extending to the south of the Península de Valdés. It can be also observed that in the mouths of the Nuevo and San Matías gulfs there are areas where there is the potential to break stratification. These results are qualitatively consistent with those obtained by Palma, Matano, and Piola (2004) from numerical simulations with a lower resolution model.

A comparison of the fronts observed on the Patagonian Shelf from satellite sea surface temperature data (Palma, Matano, and Piola, 2004; Pisoni and Rivas, 2006) with those computed with the use of the Simpson-Hunter parameter in our simulations suggests that most of the fronts that occur along the coast have their origin in the vertical mixing produced by the tides. Those fronts are associated with regions of high chlorophyll *a* concentration (Romero *et al.*, 2006), suggesting the importance of frontal processes for fisheries. They have also been related to the exchange of CO_2 between the ocean and the atmosphere (Bianchi *et al.*, 2005).

SUMMARY AND CONCLUSIONS

The aim of this paper has been to study the propagation of the tide from the Patagonian Shelf to the North Patagonia Gulfs, using a set of three nested models based on the HamSOM model code. The model is three dimensional, allowing for a better representation of bottom currents and, therefore, of bottom friction, and the grids utilized are of high resolution (up to 1 km) and include the best bathymetry and coastline data available. These simulations represent a significant improvement over previously published works for the region and over global models. For instance, even the FES2004 model (Lyard *et*

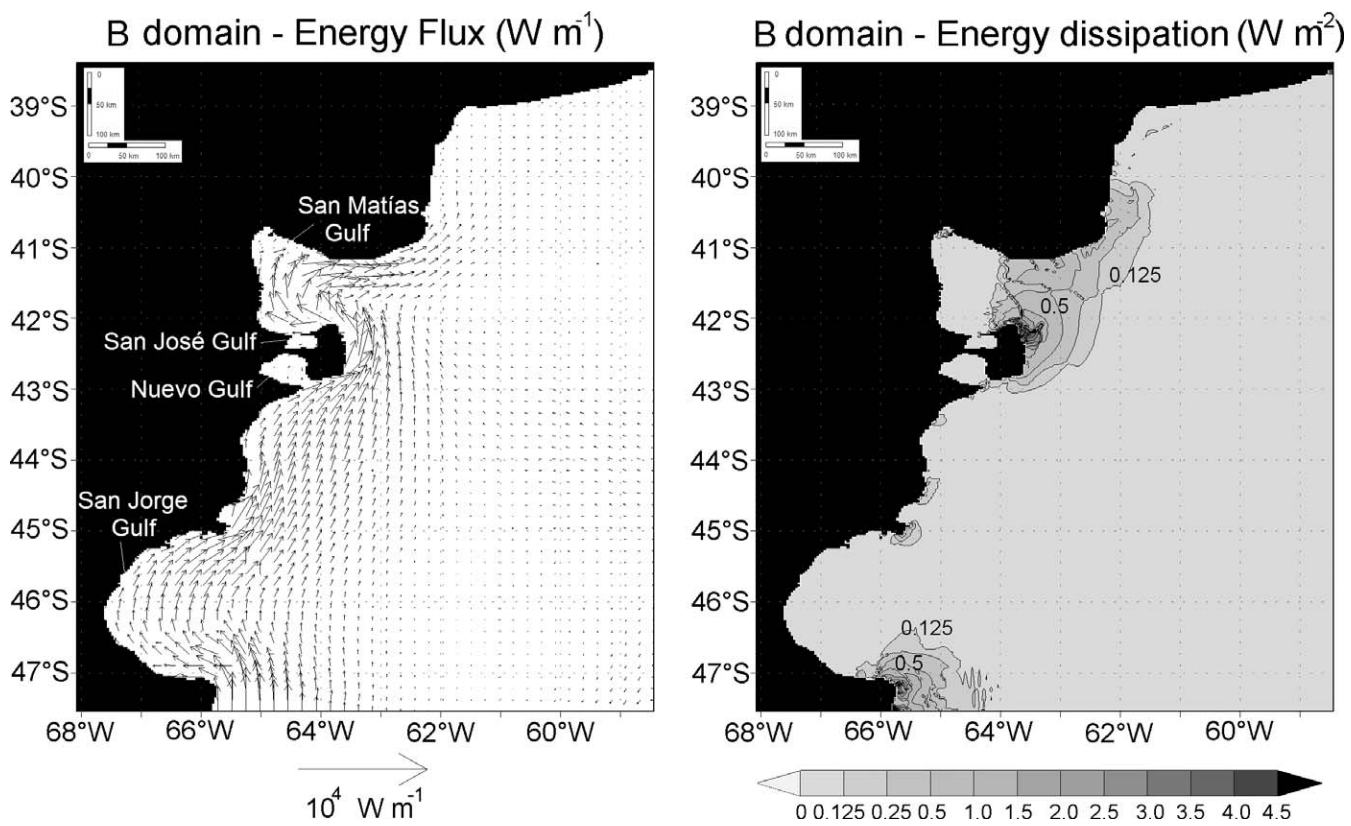

Figure 10. M_2 tidal energy flux vectors in W m^{-1} (left panel) and contours of tidal energy dissipation by bottom friction in W m^{-2} (right panel) derived from model B. Note that the contour interval is not regular.

al., 2006), with a 1/8° resolution does not properly represent the small North Patagonia Gulfs. San José Gulf is represented by only four aligned points, the Nuevo Gulf by around a dozen points, and the gulfs' mouths are limited to the width of one grid point. As a consequence, the error in the estimation of the tidal constituent in that model is quite large; for instance the M_2 amplitude in Puerto Madryn has an error of 17%. On the other hand, tidal currents, which are very sensitive to the coastline and bathymetry, cannot be well resolved in those areas.

Simulations were validated using the available tidal gauge and tidal current observations, leading to a good correspondence. Differences in the modeled amplitudes were less than 10% in the three domains utilized, whereas differences in the phase lag were less than 30° for the lowest resolution model and less than 17° for the other two higher resolution domains. The correspondence between modeled and observed tidal currents was very acceptable, showing that the model is able to capture the main features of both the amplitude and the direction of the tidal ellipses. Even though we have limited the discussion to M_2, our results indicate that the model simulates the most important diurnal and semidiurnal constituents with accuracy similar to that constituent. Therefore, we believe that the simulation can be employed in other areas where observations are not available and that the models can provide a useful management tool.

The simulations allowed the construction of higher resolution and more reliable cotidal and corange charts for the North Patagonia Gulfs. The generation of higher order harmonics by nonlinear effects was also analyzed. Maximum values in the North Patagonia Gulfs occur in the Nuevo Gulf, in which the M_4 amplitude always exceeds 0.12 m, and in the area of San Antonio in San Matías Gulf. In our simulations M_4 was not included as a boundary condition in the largest scale coarser resolution model. Nevertheless, the FES 2004 global model suggests that there the amplitude of this constituent is small, with values less than 1 cm along the eastern boundary and on the order of 1 mm along the southern one. Therefore, M_4 in the area is mostly locally generated, and our results probably represent the actual values. This seems to be confirmed by the few observations available.

Currents in San Matías gulf are found to be much larger toward the mouth, and maximum speed, exceeding two to three time the values in the interior, occurs northeast of the Península de Valdés and east of Caleta Valdés, representing a significant energy source for vertical mixing.

The energy flux and the energy dissipation by bottom friction were computed for the three domains; the highest resolution simulations permitted the first estimations of those magnitudes for the North Patagonia Gulfs. Results indicate that dissipation in the area constitutes an important part (around

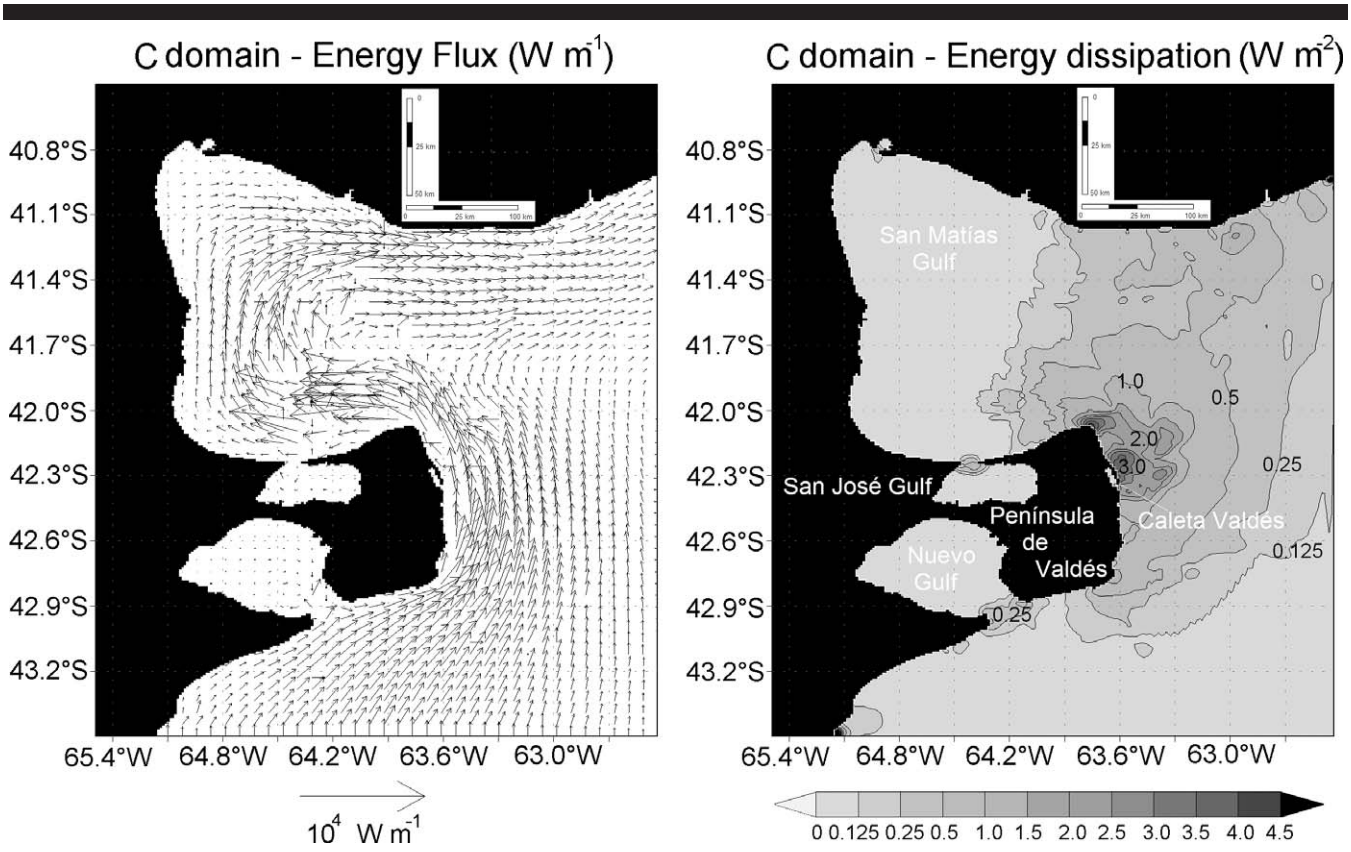

Figure 11. M_2 tidal energy flux vectors in W m^{-1} (left panel) and contours of tidal energy dissipation by bottom friction in W m^{-2} (right panel) derived from model C. Note that the contour interval is not regular.

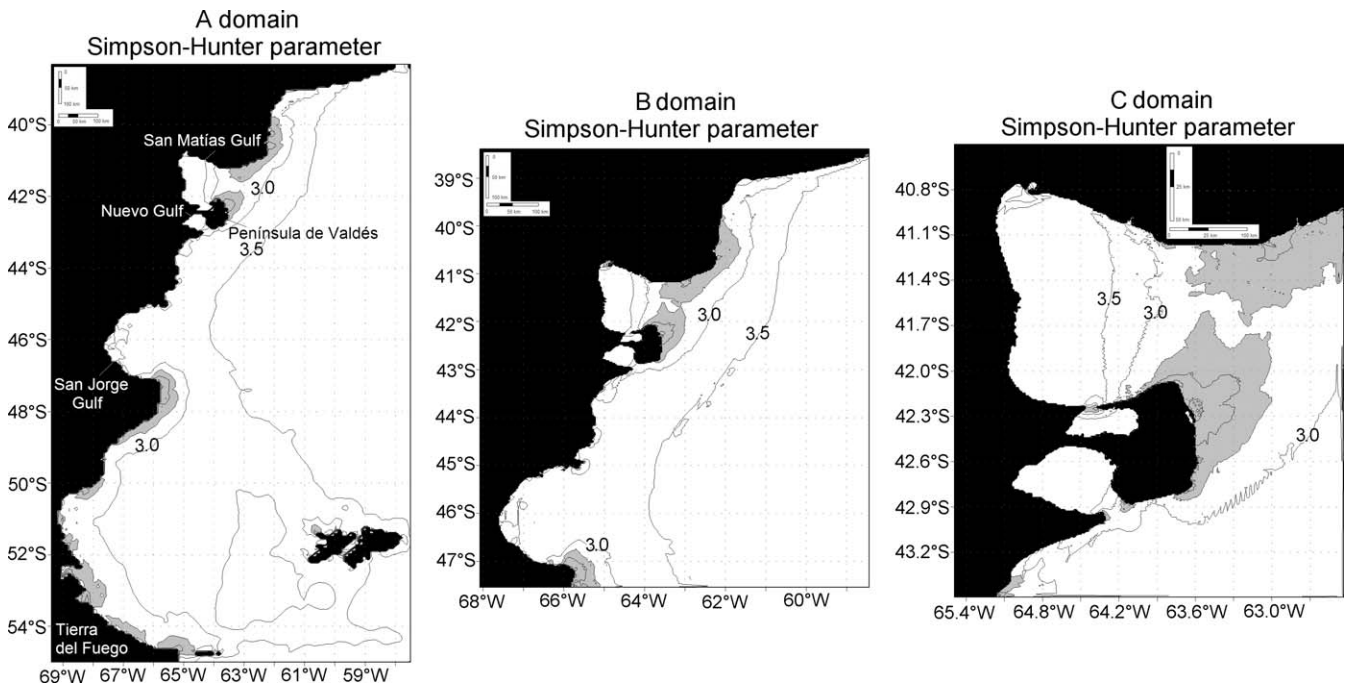

Figure 12. Contours of the Simpson-Hunter parameter from models A (left panel), B (central panel), and C (right panel). Areas where the parameter is less than 2.5 have been shaded.

17%) of the total energy dissipated in the Patagonian Shelf which, in turn, is one of the most dissipative regions of the world ocean. Most of the dissipation occurs at the mouths of the gulfs and especially northeast of the Península de Valdés and east of Caleta Valdés.

The Simpson-Hunter parameter derived from the simulations indicates that at the mouths of the three North Patagonia Gulfs the tide has enough kinetic energy to overcome stratification and produce tidal fronts. The most significant areas are located at the mouth of San Matías Gulf and east of the Península de Valdés in good agreement with observations of thermal fronts (Pisoni and Rivas, 2006). Those fronts are related to areas of high primary production (Pisoni and Rivas, 2006; Romero *et al.*, 2006; Sabatini, 2004) and, therefore, are important for fisheries in the region.

Finally, even though the results presented in this paper have significantly improved our understanding of tidal dynamics in this region, the collection of more observations, particularly in the interior and at the mouths of the three gulfs, is necessary to complete the validation of the results here discussed.

ACKNOWLEDGMENTS

This paper is a contribution to the UNDP Project ARG/02/018—GEF BIRF No. 28385-AR "Prevention of coastal contamination and management of the marine biodiversity" and the Subproject A-B-30 "Study of the circulation in the San Matías Gulf with numerical models forced by tides and winds" and the UBA Grant I014.

LITERATURE CITED

Accad, Y. and Pekeris, C.L., 1978. Solution of the tidal equations for the M2 and S2 tides in the world oceans from a knowledge of the tidal potential alone. *Philosophical Transactions of the Royal Society, Series A*, 290, 235–266.

Alvarez Fanjul, E.A.; Pérez Gómez, B., and Rodríguez Sanchez-Arévalo, I., 1997. A description of the tides in the Eastern North Atlantic. *Progress in Oceanography*, 40, 217–244.

Backhaus, J.O., 1983. A semi-implicit scheme for the shallow water equations for application to shelf sea modelling. *Continental Shelf Research*, 2(4), 243–254.

Backhaus, J.O., 1985. A three dimensional model for simulation of shelf sea dynamics. *Deutsche Hydrographische Zeitschrift*, 38(H.4), 164–187.

Backhaus, J.O. and Hainbucher, D., 1987. A finite difference general circulation model for shelf sea and its applications to low frequency variability on the North European Shelf. *In:* Nihoul, J.C. and Jamars, B.M. (eds.), *Three Dimensional Model of Marine and Estuarine Dynamics*. Elsevier Oceanographic Series 45. Amsterdam: Elsevier, pp. 221–244.

Bava, J.; Gagliardini, D.A.; Dogliotti, A.I., and Lasta, C.A., 2002. Annual distribution and variability of remotely sensed sea surface temperature fronts in the Southwestern Atlantic Ocean. Twenty-ninth International Symposium on Remote Sensing of Environment, April 8–12, 2002 (Buenos Aires, Argentina).

Bianchi, A.A.; Bianucci, L.; Piola, A.R.; Pino, D.R.; Schloss, I.; Poisson, A., and Balestrini, C.F., 2005. Vertical stratification and air-sea CO_2 fluxes in the Patagonian shelf, *Journal of Geophysical Research*, 110, C07003, doi:10.1029/2004JC002488.

Borjas, R.D.V. and Dragani, W.C., 2004. Generación de batimetrías digitales para la modelación matemática de la circulación oceánica costera en Patagonia. XXII Reunión Científica de Geofísica y Geodesia. September, 6–10, 2004 (Buenos Aires, Argentina) [in Spanish].

Bos, M.S. and Scherneck, H.G., 2008. Free ocean tidal loading provider. Onsala Space Observatory. http://www.oso.chalmers.se/~loading/index.html (accessed September 17, 2009).

Cartwright, D.E. and Ray, R.D., 1989. New estimates of oceanic tidal energy dissipation from satellite altimetry. *Geophysical Research Letters*, 16(1), 73–76.

Courant, R.; Friedrichs, K., and Lewy, H., 1928. Über die partiellen Differenzengleichungen der mathematischen Physik. *Mathematische Annalen*, 100(1), 32–74 [in German].

Davies, A.M.; Sauvel, J., and Evans, J., 1985. Computing near coastal tidal dynamics from observations and a numerical model. *Continental Shelf Research*, 4(3), 341–366.

Egbert, G.D. and Ray R.D, 2000. Significant dissipation of tidal energy in the deep ocean inferred from satellite altimeter data. *Nature*, 405, 775–778.

Foreman, M.G.G., 1977. Manual for Tidal Heights Analysis and Prediction. Patricia Bay, Sidney, B.C., Canada: Institute of Ocean Science, Pacific Marine Science Report 77–10, 97p.

Foreman, M.G.G., 1978. Manual for Tidal Currents Analysis and Prediction. Patricia Bay, Sidney, B.C., Canada: Institute for Ocean Sciences, Pacific Marine Science Report 78-6, 65p.

Framiñan, M.B., Balestrini, C.F.; Bianchi, A.A.; Demilio, G., and Piola, A.R., 1991. Datos CTD, series temporales de velocidad, temperatura y conductividad en el Golfo San Matías. Departamento Oceanographia. Servicio de Hidrografía Naval, Informe Técnico No. 63/1991, Argentina [in Spanish]. 41p.

Francis, O. and Mazzega, P., 1990. Global charts of ocean tide loading effects. *Journal of Geophysical Research*, 95(C7), 11411–11424.

Gagliardini, D.A. and Rivas, A.L., 2004. Environmental characteristics of San Matías Gufl obtained from LANDSAT-TM and ETM+ data. *Gayana (Concepción)*, 68(2), 186–193.

Glorioso, P.D., 1987. Temperature distribution related to shelf-sea fronts on the Patagonian shelf. *Continental Shelf Research*, 7(1), 27–34.

Glorioso, P.D., 2000. Patagonian Shelf 3-D tide and surge model. *Journal of Marine Systems*, 24, 141–151.

Glorioso, P.D. and Flather, R.A., 1995. A barotropic model of the currents off SE South America. *Journal of Geophysical Research*, 100, 13427–13440.

Glorioso, P.D. and Flather, R.A., 1997. The Patagonian Shelf tides. *Progress in Oceanography*, 40, 263–283.

Glorioso, P.D. and Simpson, J.H., 1994. Numerical modelling of the M2 tide on the northern Patagonian shelf. *Continental Shelf Research*, 14, 267–278.

Hearn, C.J., 1985. On the value of the mixing efficiency in the Simpson-Hunter h/u^3 criterion. *Ocean Dynamics*, 38(3), 133–145.

Lefèvre F; Le Provost, C., and Lyard, F.H., 2000. How can we improve a global ocean tide model at a regional scale? A test on the Yellow Sea and the East China Sea. *Journal of Geophysical Research*, 105 (C4), 8707–8725.

Lefèvre F; Lyard, F.H.; Le Provost, C., and Schrama, E.J.O., 2002. FES99: a global tide finite element solution assimilating tide gauge and altimetric information, *Journal of Atmospheric and Oceanic Technology*, 1345–1356.

Le Provost, C. and Lyard, F., 1997. Energetics of the semi-diurnal M2 ocean tide. *Progress in Oceanography*, 40, 37–52.

Le Provost C; Lyard, F.; Genco, M.L., and Rabilloud, F., 1998. A hydrodynamic ocean tide model improved by assimilation of a satellite altimeter-derived data set. *Journal of Geophysical Research*, 103(C3), 5513–5529.

Lyard, F., 1999. Data assimilation in a wave equation: a variational representer approach for the Grenoble tidal model. *Journal of Computational Physics*, 149, 1–31.

Lyard, F.; Lefèvre, F.; Letellier, T., and Francis, O., 2006. Modelling the global ocean tides: modern insights from FES2004. *Ocean Dynamics*, 56, 394–415.

Mazio, C.A., 2006. Estructura mareologica en Norpatagonia utilizando el modelo Wqmap. *Geoacta*, 31:109–115 [in Spanish].

Mazio, C.A.; Dragani, W.C.; Caviglia, F.J., and Pousa, J.L., 2004. Tidal hydrodynamics in Golfo Nuevo, Argentina, and the adjacent continental shelf. *Journal of Coastal Research*, 20(4), 1000–1011.

Miller, G.R., 1966. The flux of tidal energy out of the deep oceans. *Journal of Geophysical Research*, 71, 2485–2489.

Moreira, D.; Simionato, C.G.; Dragani, W.C., and Nuñez, M.N., 2009. Tidal and residual currents observations at the San Matías and San José gulfs, Northern Patagonia, Argentina. *Journal of Coastal Research*, 25(4), 957–968, doi:10.2112/08–1035.

Munk, W., 1997. Once again: once again—tidal friction. *Progress in Oceanography*, 40, 7–35.

O'Donnell, J., 1993. Surface fronts in estuaries: a review. *Estuaries*, 16(1), 12–39.

Palma, E.D.; Matano, R.P., and Piola, A.R., 2004. A numerical study of the southwestern Atlantic Shelf circulation: barotropic response to tidal and wind forcing, *Journal of Geophysical Research*, 109, C08014, doi:10.1029/2004JC002315.

Pisoni, J.P. and Rivas, A., 2006. Frentes térmicos sobre la PCA por medio de imágenes satelitales. Proceedings of the VI Jornadas Nacionales de Ciencias del Mar and XIV Coloquio de Oceanografía. December, 4–8, 2006. Puerto Madryn, Argentina [in Spanish].

Pugh, D.T., 1987. Tides, Surges and Mean Sea-Level: A Handbook for Engineers and Scientists. Chichester, UK: Wiley, 472p.

Rivas, A.L. and Beier, E.J., 1990. Temperature and salinity fields in the Northpatagonic gulfs. *Oceanologica Acta*, 13, 15–20.

Rivas, A.L. and P. Dell'arciprete, 2000. Frentes térmicos en la plataforma Patagónica inferidos a partir de datos satelitales. IV Jornadas Nacionales de Ciencias del Mar, September 18–22, 2000, Puerto Madryn, Argentina [in Spanish].

Romero, S.I.; Piola, A.R.; Charo, M., and Garcia, C.A.E., 2006. Chlorophyll-a variability off Patagonia based on SeaWiFS data. *Journal of Geophysical Research*, 111, C05021, doi:10.1029/2005JC003244.

Sabatini, M.E., 2004. Características ambientales, reproducción y alimentación de la merluza (Merluccius hubbsi) y la anchoíta (Engraulis anchoíta) en su hábito reproductivo patagónico. Síntesis y perspectivas. *Revista de Investigación y Desarrollo Pesquero*, 16, 5–25 [in Spanish].

SHN (Servicio de Hidrografía Naval), 2000. Derrotero Argentino Parte II. Costa del Atlántico. Desde Cabo San Antonio a Cabo Vírgenes y Punta Dungeness y Suplemento. 9th edition. Buenos Aires, Argentina: Servicio de Hidrografía Naval, Armada de la República Argentina, Publicación H 202 [in Spanish].

SHN, 2008. Tablas de Marea. Buenos Aires, Argentina: Servicio de Hidrografía Naval, Ministerio de Defensa, Publicación H 610 [in Spanish].

Simionato, C.G.; Dragani, W.; Nuñez, M.N., and Engel, M., 2004. A set of 3-D nested models for tidal propagation from the Argentinean Continental Shelf to the Río de la Plata estuary—Part I M_2. *Journal of Coastal Research*, 20(3), 893–912.

Simpson, J.H. and Hunter, J., 1974. Fronts in the Irish Sea. *Nature*, 250, 404–406.

SOGREAH (Societé Grenobloise d'Etudes et Applications Hydrauliques), 1959. Proyecto de usina mareomotríz em el Golfo San José (Península Valdés) (Misión Hidrográfica). Contrato entre la Dirección Nacional de Energía y la Societé Grenobloise d'Etudes et Applications Hydrauliques (France), 70p.

UNDP (United Nations Development Program, 2002. Prevention of Coastal Contamination and Management of the Marine Biodiversity. Project ARG/02/018-GEF BIRF No. 28385–AR.

UNESCO (United Nations Educational, Scientific and Cultural Organization), 1999. Title. http://www.unesco.org/whc/sites/937.htm (accessed September 17, 2009).

Wessel, P. and Smith, W.H.F., 1996. A global self-consistent, hierarchical, high-resolution shoreline database. *Journal of Geophysical Research*, 101(B4), 8741–8743.

Woodworth, P.L.; Pugh, D.T.; Meredith, M.P., and Blackman, D.L., 2005. Sea level changes at Port Stanley, Falkland Islands. *Journal of Geophysical Research*, 110, C06013, doi:10.1029/2004JC002648.

Zahel, W., 1997. Ocean tides. *In:* Wilhelm, H., Zürn, W., and Wenzel, H.-G. (eds.), *Lecture Notes in Earth Sciences: Tidal Phenomena*. Berlin: Springer, 66p.

□ **SUMARIO** □

Durante la última década, los modelos de marea han mejorado espectacularmente. No obstante, aún presentan dificultades para resolver la marea sobre las plataformas continentales y cerca de la costa. En este trabajo se estudia la propagación de la marea de la Plataforma Continental a los Golfos Norpatagónicos de Argentina, aplicando un conjunto de tres modelos anidados de alta resolución basados en el modelo Hamburg Shelf Ocean Model (HamSOM), en los cuales se puso particular atención en la batimetría y la línea de costa. El estudio es complementado con el uso de todas las observaciones de marea y corriente de marea disponibles. Las simulaciones muestran buena concordancia con las observaciones, permitiendo la construcción de cartas cotidales y de isoamplitud más confiables y de mayor resolución. El régimen de marea en el área es esencialmente semidiurno y dominado por la M_2. Esta componente se propaga hacia el norte como una onda de Kelvin y alcanza los golfos desde el sur. En su interior se observa una significativa amplificación. Las corrientes de marea son grandes en las bocas de los golfos y se debilitan en su interior. Fue analizada la transferencia no lineal de energía de los armónicos diurnos a los de mayor orden. Esta puede ser muy importante en el interior de los golfos, particularmente en el Golfo Nuevo, y en la porción noroccidental del Golfo San Matías, cerca de San Antonio. Se computaron el flujo de energía y la disipación energética por fricción de fondo, que indican que esta región disipa el 17% de la energía total disipada en la Plataforma Patagónica que, a su vez, es una de las áreas más disipativas del océano. El parámetro de Simpson–Hunter calculado a partir de las simulaciones muestra que en la boca de los golfos, especialmente del San Matías y al este de la Península de Valdés, las mareas son lo suficientemente energéticas como para superar la estratificación y producir frentes de marea. Los sitios donde se localizan los frentes de marea en las simulaciones son consistentes con resultados derivados del análisis de observaciones de la temperatura superficial del mar y productividad primaria mostrados por otros autores.